RESEARCH ARTICLE | SEPTEMBER 16 2024

Elevating electron energy gain and betatron x-ray emission in proton-driven wakefield acceleration

Hossein Saberi ; Guoxing Xia ; Linbo Liang ; John Patrick Farmer ; Alexander Pukhov

Phys. Plasmas 31, 093104 (2024)
https://doi.org/10.1063/5.0216713

Elevating electron energy gain and betatron x-ray emission in proton-driven wakefield acceleration

Cite as: Phys. Plasmas **31**, 093104 (2024); doi: 10.1063/5.0216713
Submitted: 30 April 2024 · Accepted: 18 August 2024 ·
Published Online: 16 September 2024

Hossein Saberi,[1,2,a)] Guoxing Xia,[1,2,b)] Linbo Liang,[1,2] John Patrick Farmer,[3,4] and Alexander Pukhov[5]

AFFILIATIONS

[1]Department of Physics and Astronomy, University of Manchester, Manchester M13 9PL, United Kingdom
[2]Cockcroft Institute, Daresbury, Cheshire WA4 4AD, United Kingdom
[3]CERN, 1211 Geneva, Switzerland
[4]Max Planck Institute for Physics, 80805 Munich, Germany
[5]Heinrich-Heine-Universität Düsseldorf, 40225 Düsseldorf, Germany

[a)]**Author to whom correspondence should be addressed:** hossein.saberi@manchester.ac.uk
[b)]**Electronic mail:** guoxing.xia@manchester.ac.uk

ABSTRACT

The long proton beams present at CERN have the potential to evolve into a train of microbunches through the self-modulation instability process. The resonant wakefield generated by a periodic train of proton microbunches can establish a high acceleration field within the plasma, facilitating electron acceleration. This paper investigates the impact of plasma density on resonant wakefield excitation, thus influencing the acceleration of a witness electron bunch and its corresponding betatron radiation within the wakefield. Various scenarios involving different plasma densities are explored through particle-in-cell simulations. The peak wakefield in each scenario is calculated by considering a long pre-modulated proton driver with a fixed peak current. Subsequently, the study delves into the witness beam acceleration in the peak wakefield and its radiation emission. Elevated plasma density increases both the number of microbunches and the accelerating gradient of each microbunch, consequently resulting in heightened resonant wakefield. Nevertheless, the scaling is disrupted by the saturation of the resonant wakefield due to the nonlinearities. The simulation results reveal that at high plasma densities, an intense and broadband radiation spectrum extending into the domain of the hard x-rays and gamma rays is generated. Furthermore, in such instances, the energy gain of the witness beam is significantly enhanced. The impact of wakefield on the witness energy gain and the corresponding radiation spectrum is clearly evident at elevated densities.

I. INTRODUCTION

Electrons can be efficiently focused and accelerated within the plasma wakefield generated by a high-intensity driver, e.g., laser pulse,[1] electron,[2] or a proton beam,[3] due to the presence of very strong transverse and longitudinal electric wakefields. The wiggling electrons then emit electromagnetic radiation referred to as betatron radiation (BR), which is usually characterized by a high brightness, synchrotron-like broadband radiation.[4–6] The pulse duration is equivalent to that of the electron bunch, typically on the femtosecond scale, in various wakefield accelerator concepts. BR in laser–plasma accelerators has been observed experimentally in the kiloelectron volt (keV) photon energy range,[7] pursued by advanced experiments to boost the peak brightness[8,9] and expand the energy range.[10–12] Advanced single-shot phase contrast imaging with BR has been demonstrated in the experiment.[13] Furthermore, BR can serve as a nondestructive diagnostic tool for assessing electron beam parameters. As a result, betatron spectroscopy has attracted attention in various wakefield accelerator contexts.[14–21]

In contrast to laser pulses and electron beams, the proton driver maintains its energy in a plasma medium over much longer distances ranging from hundreds to thousands of meters.[22] The Advanced Wakefield Experiment (AWAKE) Run 1 (2016–2018) at CERN has successfully demonstrated the proton-driven plasma wakefield acceleration (PD-PWFA) using the Super Proton Synchrotron (SPS) proton beam.[23] Currently, the AWAKE Run 2 (2021–) is focused on achieving the generation of a multi-gigaelectron volt (GeV) electron beam while controlling its emittance, which holds potential for particle physics

experiments.[24] To mitigate the transverse filamentation instabilities,[25,26] The AWAKE deliberately operates at a density where the plasma skin depth is on the order of the radius of the SPS proton driver. The acceleration of the witness beam and the corresponding BR at this plasma density have been investigated in previous studies.[19,20] These studies demonstrated that the electron beam could be accelerated up to several GeV energies. Simultaneously, the betatron spectrum was observed in the UV to x-ray range.

Opting for a higher plasma density would necessitate a smaller proton driver radius. Research into proton-driven wakefield at high densities is less extensive compared to that conducted in the AWAKE. In a simulation study utilizing the long proton driver proposed for the RHIC-EIC project at the Brookhaven National Lab, proton beams with radii of 100 and 40 μm have been considered.[27] The results revealed a significant increase in the peak wakefield. In this study, particle-in-cell (PIC) simulations are conducted to explore the influence of various plasma densities on the resonantly driven wakefield acceleration. The peak wakefield in each scenario is determined by considering a long pre-modulated proton driver with a fixed peak current. The strong scaling observed at low densities is ultimately constrained by saturation of the wakefield growth at high densities. Subsequently, the investigation centers on electron acceleration at the peak wakefield amplitude, while also examining the corresponding radiation emission. The paper is structured as follows: Sec. II provides an overview of proton-driven wakefield. In Sec. III, the simulation model and the methodology are elucidated in detail. In Sec. IV, the results are presented and discussed. Conclusions are summarized in Sec. V.

II. PROTON-DRIVEN WAKEFIELD

The PD-PWFA concept, first proposed by Caldwell *et al.*,[28] has introduced a pioneering approach to future plasma-based colliders that could be realized within a single acceleration stage.[29] While AWAKE Run 1 has marked significant strides in advancing the realization of PD-PWFA using SPS proton beam,[23] AWAKE Run 2 aims to achieve a high quality beam suitable for applications in particle physics experiments.[24]

The geometry of the SPS beam imposes limitations on its suitability for plasma wakefield excitation. The SPS beam has a few centimeter-scale length, while it should be on the order of the plasma wavelength, i.e., sub-millimeter scale, to effectively generate wakefields in the plasma. However, this obstacle is overcome by an intrinsic plasma instability. The long proton beam undergoes self-modulation instability in the plasma, resulting in the formation of a train of microbunches with a period on the order of the plasma wavelength.[30] Although self-modulation instability is a complex phenomenon, it has undergone comprehensive examination and validation through extensive studies conducted in the AWAKE experiment.[31]

The transverse filamentation instabilities can destroy a long proton beam when it interacts with the plasma. To avert this instability, the proton beam radius, σ_{rp}, needs to be on the order of or smaller than the plasma skin depth,[32] or

$$k_p \sigma_{rp} \leq 1, \tag{1}$$

where $k_p = 2\pi/\lambda_p$, and λ_p is the plasma wavelength. In a recent study, the experimental threshold for the instability to occur in a long proton beam was reported to be approximately 1.5 plasma skin depth.[25] The normalized emittance of the SPS proton beam is 3 mm mrad, and so the beam is focused to a radius of 200 μm. In this case, a maximum plasma density of 7×10^{14} cm^{-3} is required to meet the condition outlined in Eq. (1).

Plasma density is pivotal in wakefield acceleration as it directly influences the wavebreaking limitation. Nevertheless, opting a higher plasma density would require proton driver with smaller radius as indicated by Eq. (1). For instance, a proton driver with a radius of 100 μm could be used with the plasma density of 2.8×10^{15} cm^{-3}. The maximum plasma density and the corresponding wavebreaking limit, $\mathscr{E}_{WB}$, vs the proton beam's radius are illustrated in Fig. 1.

III. SIMULATION APPROACH

The simulation study investigates witness beam acceleration and its associated radiation emission in the plasma wakefield driven by a pre-modulated proton driver. The three-dimensional quasi-static PIC code QV3D, built upon the VLPL code platform,[33] is employed. The code incorporates a built-in module to calculate the synchrotron radiation for each macroparticle. The photons emitted by a macroparticle is calculated self-consistently from its transverse momentum change in each time step. The momentum of the macroparticle is then updated according to the energy loss to consider the influence of the radiation reaction. The output of the code is the integrated critical photon spectrum per spatial angle. One should reconstruct BR by a convolution of the output with the universal function of synchrotron radiation.[20]

We consider a baseline plasma density and three specific cases featuring higher plasma densities. The baseline scenario includes a plasma density of 7×10^{14} cm^{-3} and a proton driver with a radius of 200 μm. Three other cases are considered with proton driver radii of 150 μm (case I), 100 μm (case II), and 50 μm (case III). It should be noticed that the proton beam radius in each scenario corresponds to the plasma skin depth specific to that scenario. Plasma parameters are summarized in Table I.

A. Peak wakefield

The self-modulation process within the plasma divides a long proton beam into short microbunches, each spaced by the plasma wavelength. These microbunches resonantly excite a substantial wakefield,[30] a phenomenon demonstrated in both the AWAKE experiment[31] and simulations conducted at higher plasma densities.[27]

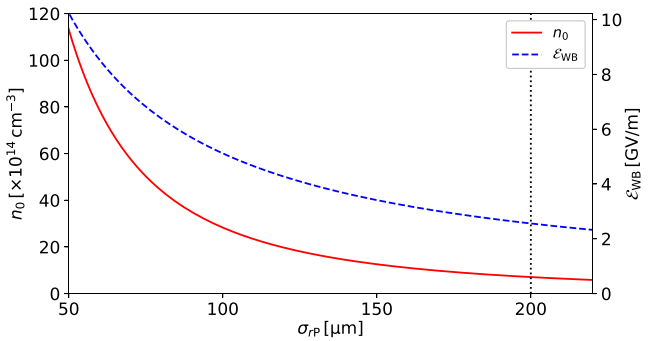

FIG. 1. Maximum plasma density and the corresponding wavebreaking limit vs the proton beam radius, ensuring prevention of beam filamentation. The dotted line indicates the SPS beam radius.

TABLE I. Parameters for the simulation study considering a baseline scenario and three distinct cases with higher plasma densities.

	Symbol (unit)	Baseline	Case I	Case II	Case III
Plasma					
Skin depth	k_p^{-1} (μm)	200	150	100	50
Density	n_0 (cm^{-3})	7×10^{14}	1.25×10^{15}	2.80×10^{15}	1.13×10^{16}
Length	L (m)	10	10	10	10
Pre-modulated driver					
Charge	Q (nC)	2.59	2.59	2.59	2.59
Length	L_d (mm)	32.8	32.8	32.8	32.8
Number of microbunches	⋯	26	34	52	104
Microbunch's length	$\sigma_{\xi mb}$ (μm)	283	213	142	71
Microbunch's radius	σ_{rmb} (μm)	200	150	100	50
Microbunch's charge	Q_{mb} (pC)	100	76	50	25

In this context, rather than conducting a full PIC simulation of the self-modulation of a long proton beam, we provide an estimation of the peak wakefield through the utilization of a pre-modulated proton driver. For all scenarios, we consider a pre-modulated proton beam comprising 1.62×10^{10} protons, spanning a full length of 32.8 mm. The beam is structured as a periodic sequence of microbunches, with a period equal to the relevant plasma wavelength. The charge is chosen to ensure that in baseline, the pre-modulated driver generates a peak wakefield of 450 MV/m.[20,34] This simplified model provides a driver with a fixed peak current that makes the comparative simulation reasonable.

We assume identical Gaussian microbunches with equal charges inside the pre-modulated driver to facilitate the estimation of its peak wakefield. Adhering to the criterion in Eq. (1), the maximum radius is utilized for microbunches in each scenario. The number of microbunches can be determined through a straightforward algebraic calculation. For instance, in the baseline scenario, 26 microbunches are present with a spacing equivalent to the plasma wavelength. The length of each microbunch is chosen as

$$k_p \sigma_{\xi mb} = \sqrt{2}, \tag{2}$$

to maximize the wakefield.[35] Here, $\sigma_{\xi mb}$ represents the length of each microbunch. The parameters of the pre-modulated driver are summarized in Table I.

The density of each microbunch is much smaller than the plasma density; therefore, the peak wakefield can be estimated using the linear theory formula as[35]

$$\mathscr{E}_{mb}[\mathrm{MV/m}] = 240 \left(\frac{N_{mb}}{4 \times 10^{10}} \right) \left(\frac{600\,\mu\mathrm{m}}{\sigma_{\xi mb}} \right)^2, \tag{3}$$

where N_{mb} is the number of protons in each microbunch. In the linear regime, we can assume a linear superposition of the wakefields to calculate the peak wakefield of the pre-modulated proton driver.

The peak wakefield can also be determined using the QV3D code by configuring the pre-modulated driver in the plasma for each scenario outlined in Table I. The simulation window in the transverse direction has a dimension of $5k_p^{-1}$. Its length, however, depends on the driver's dimensionless size. The number of macroparticles per cell for plasma and the proton beam is 4 and 1, respectively.

Figure 2 depicts the periodic train driver and the wakefield in various scenarios. The green dashed lines in Figs. 2(a)–2(c) make it evident that the wakefields of microbunches superimpose linearly reaching a maximum at the end. The notable rise in the peak wakefield at elevated plasma densities can be attributed to both the augmented number of microbunches and the heightened wakefield of each microbunch. In Fig. 2(d), the wakefield grows up to a certain point and then saturates. This observation aligns with the understanding that the wakefield of a train of microbunches may decay at some point due to the plasma nonlinearities, i.e., the nonlinear elongation of the wave period that leads to the de-phasing between the microbunches and the wakefield.[36] In Fig. 2(d), the saturated wakefield exhibits a renewed increase due to the linear superposition of the remaining microbunches within the driver. It is shown that one can periodically load a resonantly driven wakefield to prevent the nonlinear dephasing effect.[37] The wakefield peaks after the final microbunch in Figs. 2(a)–2(c), and within the driver at the end point of the linear regime in Fig. 2(d). Table II summarizes the peak wakefield of the pre-modulated driver calculated by QV3D, $\mathscr{E}_{peak}$, and using the linear theory formula, $\mathscr{E}_{LT}$, and the wavebreaking limit, $\mathscr{E}_{WB}$ for different scenarios.

It is noteworthy that in the AWAKE experiment, as the modulated proton driver travels within the plasma, the amplitude of the wakefield decays after reaching saturation. It is proposed that introducing a density step into the plasma helps the wakefield maintain a near-saturation amplitude for an extended distance along the plasma.[38]

B. Witness beam acceleration in peak wakefield

We employ a simulation model introduced by Olsen *et al.*[34] to investigate the electron beam acceleration in the peak wakefield of the pre-modulated drivers in Sec. III A. The simulation model comprises a short proton bunch as the driver and a trailing witness electron beam moving in the background plasma. The proton mass of the driver is multiplied by 10^6 and the emittance is set to zero, to render the proton driver highly rigid regardless of the beam radius, and hence neglect the wakefield variation along the plasma. The dummy driver is selected in such a way that its peak wakefield mirrors that of the pre-modulated driver beam. This model is chosen to reduce the simulation size and, consequently, the computational requirements. Although the model is highly convenient, it imposes certain physical constraints. Since the

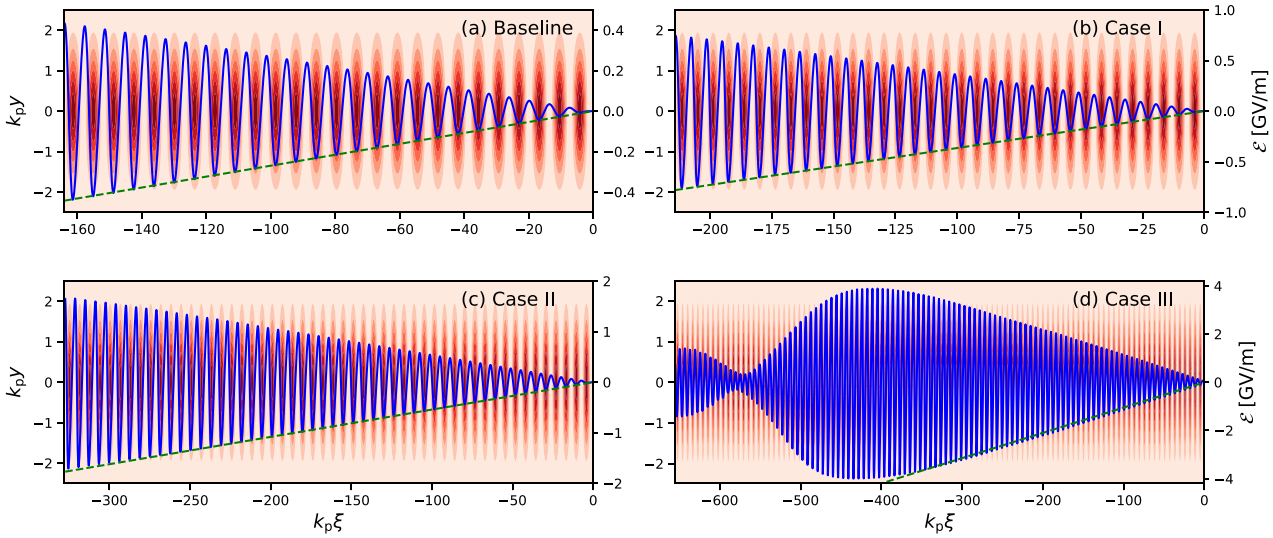

FIG. 2. The wakefield (blue line) of a train of microbunches (red contours) for baseline (a), case I (b), case II (c), and case III (d). The microbunch parameters are provided in Table I. The green dashed lines represent the linear superposition of the wakefields.

evolution of the driver is neglected, it is only appropriate in regimes in which the limiting factor on acceleration is the plasma length and not the dispersion or depletion of the driver. This would also require the emittance of the initial bunch to be scaled with the driver radius to avoid a stronger divergence for narrow beams.

With the peak wakefield identified in all scenarios, the parameters for the dummy driver in the simulation model can now be established. It shares the same radius as the train driver in each scenario. In all cases, the bunch length is assumed to be identical to that in the baseline scenario, which is 40 μm. However, the charge is optimized using QV3D simulations to align its peak wakefield with $\mathscr{E}_{\text{peak}}$ detailed in Table II. The charge will then be very high, comparable to the charge of the entire pre-modulated driver. It is important to note that the dummy driver should maintain a relatively small density, specifically $n_{\text{P}}/n_0 \lesssim 1$, to ensure its operation within the quasi-linear regime.[39]

The witness bunch radius at the entrance of the plasma must be adjusted to ensure that the witness emittance pressure matches the focusing force from its blowout. This adjustment prevents beam radius oscillation and consequently controls emittance growth.[40,41] For a Gaussian electron beam, the matched radius is determined by[34]

$$\sigma_{re} = \left(\frac{2\varepsilon_{\text{ne}}^2}{\gamma_e k_{\text{p}}^2}\right)^{1/4}, \tag{4}$$

TABLE II. The peak wakefield of the pre-modulated driver calculated by QV3D, $\mathscr{E}_{\text{peak}}$, and using the linear theory formula, $\mathscr{E}_{\text{LT}}$, and the wavebreaking limit, $\mathscr{E}_{\text{WB}}$.

	$\mathscr{E}_{\text{peak}}$ (GV/m)	$\mathscr{E}_{\text{LT}}$ (GV/m)	$\mathscr{E}_{\text{WB}}$ (GV/m)	$\mathscr{E}_{\text{peak}}/\mathscr{E}_{\text{WB}}$ (%)
Baseline	0.45	0.44	2.55	18
Case I	0.76	0.77	3.40	22
Case II	1.71	1.73	5.09	34
Case III	3.9	7.00	10.22	38

where ε_{ne} and γ_e represent the normalized emittance and the Lorentz factor of the witness beam, respectively. This results in distinct beam radii for each scenario. The beam length should be less than $\lambda_{\text{p}}/4$ to ensure that the witness beam remains in the accelerating phase of the wakefield. As a result, $k_{\text{p}}\sigma_{\xi\text{e}}$ is chosen to be constant in all scenarios. This leads to shorter witness lengths at higher plasma densities. The witness charge is carefully chosen using QV3D simulation to ensure consistent beam loading in each scenario. This configuration ensures that the entire bunch experiences an almost identical electric field, leading to collective acceleration and the production of a quasi-monoenergetic beam with minimal energy spread. The distinct nature of case III leads to a dual reduction in the witness charge, first due to its shorter length and secondarily because of its lower current that stems from saturation.

C. Simulation configuration

PIC simulations are conducted by defining a simulation window of dimensions $(11, 5, 5) \times k_{\text{p}}^{-1}$ in the $(\xi, \text{y}, \text{z})$ directions. Here, ξ denotes the longitudinal direction, and y and z represent the transverse directions. A spatial resolution of $(0.1, 0.05, 0.05) \times k_{\text{p}}^{-1}$ and a time step of $5\omega_{\text{p}}^{-1}$ are considered in all scenarios. The number of macroparticles per cell for the plasma, driver, and witness beams are set at 4, 1, and 16, respectively. A spatial delay of $k_{\text{p}}\xi = 6$ is introduced between the witness and driver beams to ensure that the witness beam is in the accelerating phase of the wakefield. The parameters for the dummy driver and the witness beam in all scenarios are summarized in Table III.

In Fig. 3, the wakefield (blue line), the beam-loaded wakefield (dashed blue line), and the driver and witness beams are depicted for baseline (a), case I (b), case II (c), and case III (d), respectively. It is evident that the maximum unloaded wakefields align with the $\mathscr{E}_{\text{peak}}$ as outlined in Table II. On the other hand, the loaded wakefields exhibit near uniform fields, facilitating the acceleration of the witness beam in a quasi-monoenergetic manner. A comparative plot of the drivers'

TABLE III. Parameters for simulation of the witness beam acceleration in the wakefield of the dummy driver for various scenarios.

Parameter	Symbol (unit)	Baseline	Case I	Case II	Case III
Dummy driver					
Energy	E_P (GeV)	400	400	400	400
Charge	Q_P (nC)	2.34	2.37	2.51	2.02
Density	n_P/n_0	0.83	0.83	0.88	0.71
Bunch length	$\sigma_{\xi P}$ (μm)	40	40	40	40
Bunch radius	σ_{rP} (μm)	200	150	100	50
Electron witness					
Energy	E_e (MeV)	150	150	150	150
Charge	Q_e (pC)	120	115	113	64
Density	n_e/n_0	34.1	32.7	32.3	18.1
Bunch length	$\sigma_{\xi e}$ (μm)	60	45	30	15
Bunch radius	σ_{re} (μm)	5.75	4.98	4.07	2.87
Energy spread	δE_e(%)	0.1	0.1	0.1	0.1
Normalized emittance	ε_{ne} (mm rad)	2	2	2	2

wakefields in dimensionless units is shown in Fig. 4. The wakefields peak almost at the position of the witness beam.

IV. SIMULATION RESULTS AND DISCUSSION

We perform the simulation study of the witness beam acceleration and its associated radiation emission. The simulation window moves over 10-m plasma length. The final energy and the integrated radiation emission are analyzed for different cases.

In Fig. 5, the energy gain and energy spread of the witness beam in various scenarios are depicted. As anticipated, the energy gain is significantly enhanced with increasing plasma density. The baseline achieves 3.5 GeV with 7% rms energy spread, a result comparable to those reported in the study by Liang *et al.*[20] The simulations conducted

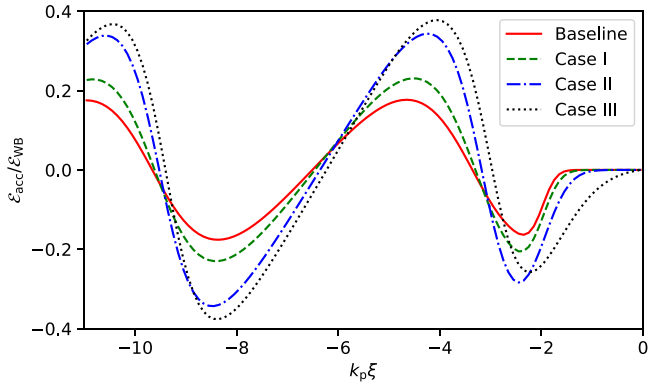

FIG. 4. Dimensionless wakefield of the dummy driver in various scenarios.

by Olsen *et al.*[34] for a similar witness beam, albeit with the initial charge and energy of 100 pC and 217 MeV, reveal a mean momentum of 1.67 GeV/c and an energy spread of 5.2% over 4 m of plasma. The simulation results here indicate an improved energy gain compared with AWAKE Run 1,[23] primarily due to the beam loading effect and the witness-matched radius. The witness beam in cases I, II, and III achieves final energies of 5.8, 12.2, and 25.9 GeV, with rms energy spreads of 7%, 9%, and 9%, respectively. The findings indicate that the plasma density is a crucial factor for resonantly driven wakefield acceleration over a restricted length. A straightforward comparison with the baseline reveals that augmenting the plasma density by a factor of 1.8 (as in case I) results in a 1.7-fold increase in energy gain. Likewise, in case II, where the plasma density increases by a factor of 4, the energy gain escalates by a factor of 3.5 compared with the baseline. In case III, with a plasma density increase by a factor of 16.1, the energy gain rises by a factor of 7.4. As previously discussed, an increase in plasma density leads to a rise in both the number of microbunches and the wakefield driven by an individual microbunch. In linear scenarios as in

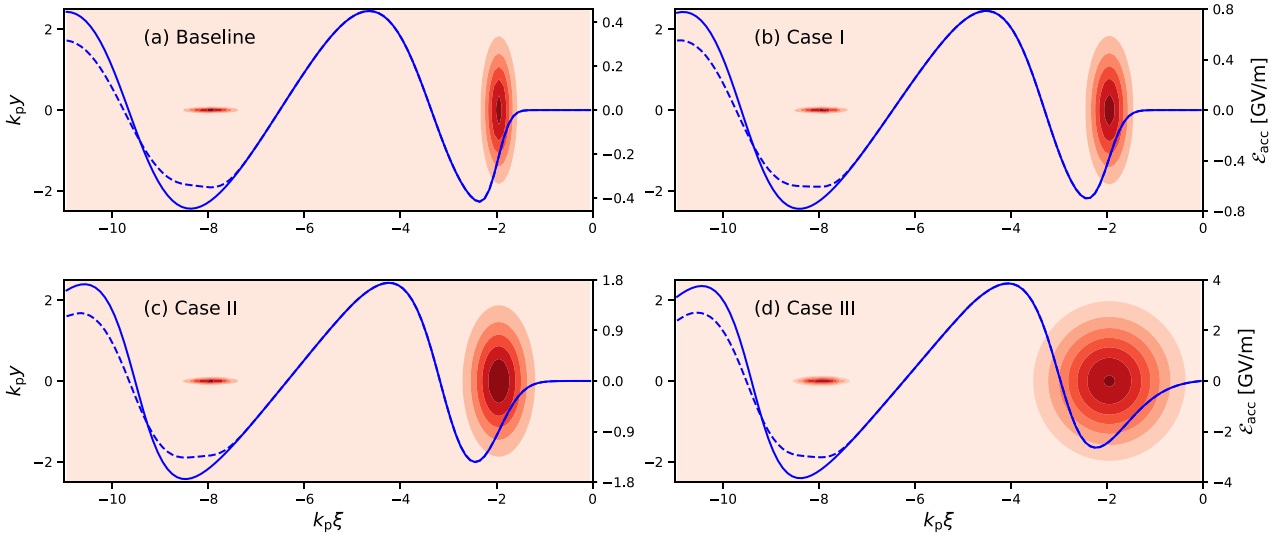

FIG. 3. The longitudinal wakefield (blue line), the beam-loaded wakefield (dashed blue line), and density contour plots of the dummy driver at $k_p\xi = -2$ and the witness beam at $k_p\xi = -8$ for baseline (a), case I (b), case II (c), and case III (d). Parameters are detailed in Table III.

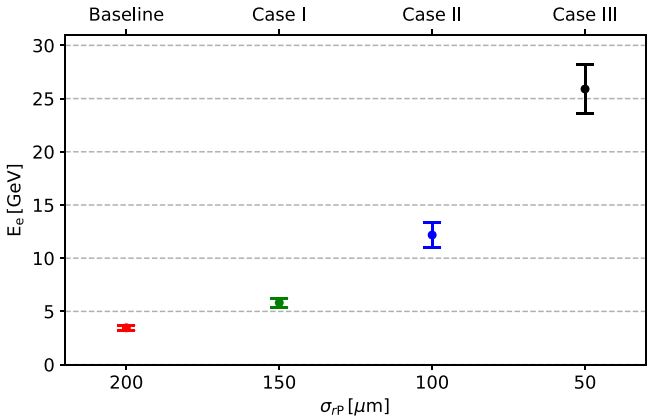

FIG. 5. Final energy of the witness beam along with the corresponding rms energy spread for various scenarios outlined in Table III.

baseline, case I, and case II, this results in an accelerating field proportional to ω_p^2, i.e., the plasma density. However, upon reaching saturation as in case III, the benefit of "more microbunches" diminishes since the wakes saturate after a certain number of microbunches. Nevertheless, the wake driven by one single microbunch still remains higher, resulting in a scaling of wakefield approximately proportional to ω_p, i.e., $\sqrt{n_p}$.

Figure 6 displays the witness beam radiation spectra for the baseline and three distinct cases of higher plasma densities. The spectra are integrated over the 10-m plasma length. The radiation spectrum of the baseline is primarily in the UV to low-energy x-ray range, featuring a critical energy of $E_c = 302$ eV. The critical photon energy of the bunch is calculated as: $E_c = 15\sqrt{3}\langle E\rangle/8$, where $\langle E\rangle$ is the mean photon energy of the spectrum. At the critical energy, half of the radiated energy is below it and the other half is above. The simulation results indicate the critical energies of 1.1, 9.0, and 91.1 keV for case I, case II, and case III, respectively. The spectrum spans more broadly into the hard x-ray to the gamma ray range as the plasma density elevated. It is noticeable that the spectrum in case III starts from a lower photon number. This different behavior originates from the reduction in the witness charge in this scenario.

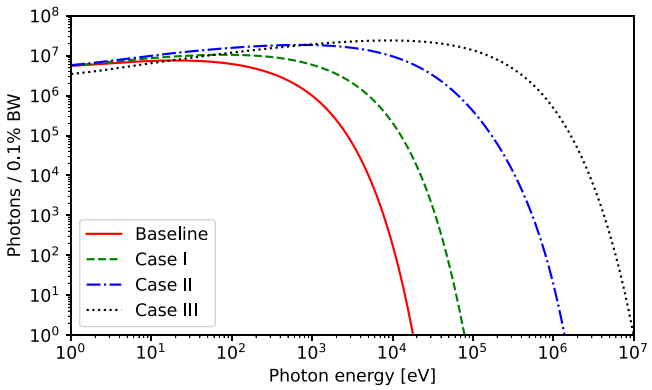

FIG. 6. Betatron spectra for various scenarios outlined in Table III.

The critical photon energies for all scenarios are shown in Fig. 7(a). Additionally, the total photon numbers can be calculated as 3.9×10^9 in baseline, 2.2×10^{10} in case I, 3.8×10^{11} in case II, and 5.2×10^{12} in case III. Figure 7(b) depicts the total photon numbers in all scenarios. The critical energy and total photons increase more sharply in case II and case III compared to those in case I as the plasma density rises more rapidly. In the simulations, the angular photon distribution with respect to the axial angle θ is calculated for each macroparticle. The results show that the radiation is highly collimated, with an angular spread measured in milliradians (mrad), in all scenarios. One can calculate the average angular photon distribution as $\bar{\theta} = \Sigma\theta N(\theta)/\Sigma N(\theta)$, where $N(\theta)$ is photons per angle. Figure 7(c) shows the average angular photon distribution, demonstrating that the radiation becomes more collimated at higher plasma densities as the beam energy increases. Although the radiation divergence is

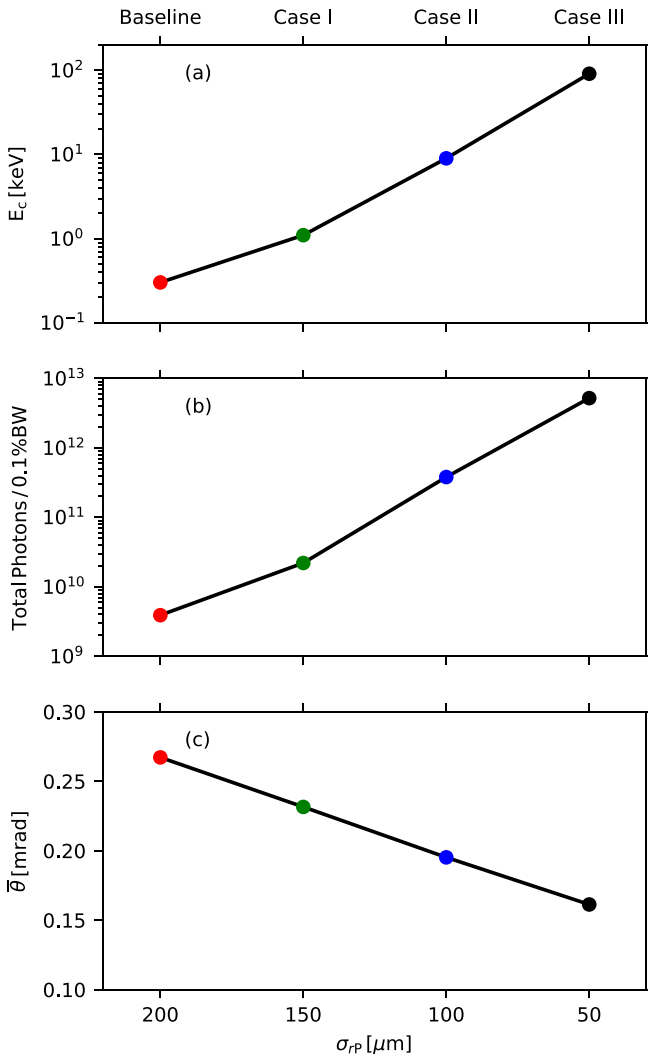

FIG. 7. Critical photon energy (a), total photon number (b), and the average angular photon distribution (c) of the BR for various scenarios.

proportional to $1/\gamma$, the decrease appears linear with a gentle slope at such highly relativistic energies.

The pulse duration of the BR will be on the order of the witness beam length. In other words, the pulse duration can be estimated as 200, 150, 100, and 50 fs for baseline, case I, case II, and case III, respectively.

X-ray sources based on laser wakefield acceleration typically operate at much higher plasma densities, around 10^{18} cm^{-3}, and over millimeter-scale distances. Recent advancements have resulted in the generation of more intense and energetic radiation, reaching critical energies of several keV.[12,42,43] Additionally, laser wakefield acceleration has recently achieved several-GeV monoenergetic beams over centimeter-long plasma acceleration,[44–46] with the most energetic electrons reaching 10 GeV.[46] On the other hand, proton beams are so energetic that they can sustain acceleration over meter-scale distances. This study demonstrates that the energy gain of the witness beam can be increased significantly, by employing higher plasma densities. This approach could lead to the generation of energetic and intense x-ray radiation at the same level or exceeding that produced by laser wakefield acceleration.

V. CONCLUSION

This paper presents a simulation study that investigates the impact of plasma density on the energy gain of the witness beam and the corresponding betatron radiation in a resonantly driven wakefield produced by a multi-microbunch driver. The peak wakefield is computed by employing a periodic train driver in four distinct scenarios of different densities. The wakefield grows until nonlinear effects occur, which leads to a subsequent decay in the wakefield. The simulation of the witness beam acceleration in the peak wakefield and its radiation emission is then presented.

The simulations demonstrate that the elevated plasma density significantly enhances electron energy gain. For instance, in case III, where the plasma density is 16 times higher, the witness beam achieves about 7.4 times higher energy compared to the baseline. Nevertheless, the nonlinear effect of wakefield decay becomes evident in case III as the energy gain scales less than ω_p^2. The findings also indicate that the elevated plasma density results in the emission of more betatron photons at higher energies. For example, in case II, the plasma density is four times that of the baseline, where the corresponding BR extends into the hard x-ray and gamma ray range, with approximately 100 times more photons per pulse. X-ray generation in a PD-PWFA is particularly valuable as a diagnostic tool. Our previous research has examined the potential of betatron diagnostic for the AWAKE project.[19,20] If higher plasma densities are employed, it becomes necessary to detect energetic photons, ranging from hard x-rays to gamma rays. It is noteworthy that the process of focusing the proton beam may require the implementation of some experimental techniques, particularly considering that it could inherently result in a broader divergence of the beam. This effect will be thoroughly explored in our forthcoming research endeavors.

ACKNOWLEDGMENTS

The authors would like to acknowledge the support from the Cockcroft Institute Core Grant No. ST/V001612/1 and the STFC AWAKE Run 2 Grant Nos. ST/T001917/1 and ST/X00614X/1.

AUTHOR DECLARATIONS

Conflict of Interest

The authors have no conflicts to disclose.

Author Contributions

Hossein Saberi: Conceptualization (lead); Investigation (lead); Methodology (lead); Software (equal); Visualization (lead); Writing – original draft (lead); Writing – review & editing (equal). **Guoxing Xia:** Conceptualization (equal); Resources (lead); Supervision (lead); Writing – review & editing (equal). **Linbo Liang:** Investigation (supporting); Methodology (supporting). **John Patrick Farmer:** Conceptualization (equal); Methodology (equal); Software (lead); Supervision (equal); Writing – review & editing (equal). **Alexander Pukhov:** Software (lead); Supervision (equal).

DATA AVAILABILITY

The data that support the findings of this study are available from the corresponding author upon reasonable request.

REFERENCES

[1]E. Esarey, C. B. Schroeder, and W. P. Leemans, "Physics of laser-driven plasma-based electron accelerators," Rev. Mod. Phys. **81**, 1229 (2009).
[2]M. J. Hogan, "Electron and positron beam-driven plasma acceleration," Rev. Accel. Sci. Technol. **9**, 63–83 (2016).
[3]E. Adli and P. Muggli, "Proton-beam-driven plasma acceleration," Rev. Accel. Sci. Technol. **9**, 85–104 (2016).
[4]E. Esarey, B. A. Shadwick, P. Catravas, and W. P. Leemans, "Synchrotron radiation from electron beams in plasma-focusing channels," Phys. Rev. E **65**, 056505 (2002).
[5]I. Kostyukov, S. Kiselev, and A. Pukhov, "X-ray generation in an ion channel," Phys. Plasmas **10**, 4818–4828 (2003).
[6]S. Wang, C. E. Clayton, B. E. Blue, E. S. Dodd, K. A. Marsh, W. B. Mori, C. Joshi, S. Lee, P. Muggli, T. Katsouleas *et al.*, "X-ray emission from betatron motion in a plasma wiggler," Phys. Rev. Lett. **88**, 135004 (2002).
[7]A. Rousse, K. T. Phuoc, R. Shah, A. Pukhov, E. Lefebvre, V. Malka, S. Kiselev, F. Burgy, J.-P. Rousseau, D. Umstadter *et al.*, "Production of a keV X-ray beam from synchrotron radiation in relativistic laser-plasma interaction," Phys. Rev. Lett. **93**, 135005 (2004).
[8]S. Kneip, C. McGuffey, J. L. Martins, S. F. Martins, C. Bellei, V. Chvykov, F. Dollar, R. Fonseca, C. Huntington, G. Kalintchenko *et al.*, "Bright spatially coherent synchrotron X-rays from a table-top source," Nat. Phys. **6**, 980–983 (2010).
[9]J. B. Svensson, D. Guénot, J. Ferri, H. Ekerfelt, I. G. González, A. Persson, K. Svendsen, L. Veisz, and O. Lundh, "Low-divergence femtosecond X-ray pulses from a passive plasma lens," Nat. Phys. **17**, 639–645 (2021).
[10]S. Cipiccia, M. R. Islam, B. Ersfeld, R. P. Shanks, E. Brunetti, G. Vieux, X. Yang, R. C. Issac, S. M. Wiggins, G. H. Welsh *et al.*, "Gamma-rays from harmonically resonant betatron oscillations in a plasma wake," Nat. Phys. **7**, 867–871 (2011).
[11]J. Ferri, S. Corde, A. Döpp, A. Lifschitz, A. Doche, C. Thaury, K. Ta Phuoc, B. Mahieu, I. A. Andriyash, V. Malka *et al.*, "High-brilliance betatron γ-ray source powered by laser-accelerated electrons," Phys. Rev. Lett. **120**, 254802 (2018).
[12]R. Rakowski, P. Zhang, K. Jensen, B. Kettle, T. Kawamoto, S. Banerjee, C. Fruhling, G. Golovin, D. Haden, M. S. Robinson *et al.*, "Transverse oscillating bubble enhanced laser-driven betatron X-ray radiation generation," Sci. Rep. **12**, 10855 (2022).
[13]S. Fourmaux, S. Corde, K. T. Phuoc, P. Lassonde, G. Lebrun, S. Payeur, F. Martin, S. Sebban, V. Malka, A. Rousse *et al.*, "Single shot phase contrast imaging using laser-produced betatron X-ray beams," Opt. Lett. **36**, 2426–2428 (2011).
[14]S. Kneip, C. McGuffey, J. L. Martins, M. S. Bloom, V. Chvykov, F. Dollar, R. Fonseca, S. Jolly, G. Kalintchenko, K. Krushelnick *et al.*, "Characterization of

transverse beam emittance of electrons from a laser-plasma wakefield accelerator in the bubble regime using betatron X-ray radiation," Phys. Rev. Accel. Beams **15**, 021302 (2012).
[15]A. Köhler, J. P. Couperus, O. Zarini, A. Jochmann, A. Irman, and U. Schramm, "Single-shot betatron source size measurement from a laser-wakefield accelerator," Nucl. Instrum. Methods Phys. Res. A **829**, 265–269 (2016).
[16]A. Curcio, M. Anania, F. Bisesto, E. Chiadroni, A. Cianchi, M. Ferrario, F. Filippi, D. Giulietti, A. Marocchino, M. Petrarca *et al.*, "Trace-space reconstruction of low-emittance electron beams through betatron radiation in laser-plasma accelerators," Phys. Rev. Accel. Beams **20**, 012801 (2017).
[17]V. Shpakov, M. P. Anania, A. Biagioni, E. Chiadroni, A. Cianchi, A. Curcio, S. Dabagov, M. Ferrario, F. Filippi, A. Marocchino *et al.*, "Betatron radiation based diagnostics for plasma wakefield accelerated electron beams at the SPARC_LAB test facility," Nucl. Instrum. Methods Phys. Res. A **829**, 330–333 (2016).
[18]P. S. M. Claveria, E. Adli, L. D. Amorim, W. An, C. E. Clayton, S. Corde, S. Gessner, M. J. Hogan, C. Joshi, O. Kononenko *et al.*, "Betatron radiation and emittance growth in plasma wakefield accelerators," Philos. Trans. R. Soc. A **377**, 20180173 (2019).
[19]B. Williamson, G. Xia, S. Gessner, A. Petrenko, J. Farmer, and A. Pukhov, "Betatron radiation diagnostics for AWAKE Run 2," Nucl. Instrum. Methods Phys. Res. A **971**, 164076 (2020).
[20]L. Liang, H. Saberi, G. Xia, J. P. Farmer, and A. Pukhov, "Characteristics of betatron radiation in AWAKE Run 2 experiment," J. Plasma Phys. **89**, 965890301 (2023).
[21]A. Curcio, A. Cianchi, G. Costa, A. D. Dotto, F. Demurtas, M. Ferrario, M. D. R. Frías, M. Galletti, J. A. Pérez-Hernández, and G. Gatti, "Reconstruction of lateral coherence and 2D emittance in plasma betatron X-ray sources," Sci. Rep. **14**, 1719 (2024).
[22]A. Caldwell and K. Lotov, "Plasma wakefield acceleration with a modulated proton bunch," Phys. Plasmas **201819**, 103101 (2011).
[23]E. Adli, A. Ahuja, O. Apsimon, R. Apsimon, A.-M. Bachmann, D. Barrientos, F. Batsch, J. Bauche, V. K. B. Olsen, M. Bernardini, AWAKE Collaboration *et al.*, "Acceleration of electrons in the plasma wakefield of a proton bunch," Nature **561**, 363–367 (2018).
[24]E. Gschwendtner, K. Lotov, P. Muggli, M. Wing, R. Agnello, C. C. Ahdida, M. C. A. Goncalves, Y. Andrebe, O. Apsimon, R. Apsimon, AWAKE Collaboration *et al.*, "The AWAKE Run 2 programme and beyond," Symmetry **14**, 1680 (2022).
[25]L. Verra, C. Amoedo, N. Torrado, A. Clairembaud, J. Mezger, F. Pannell, J. Pucek, N. van Gils, M. Bergamaschi, G. Zevi Della Porta, AWAKE Collaboration *et al.*, "Filamentation of a relativistic proton bunch in plasma," Phys. Rev. E **109**, 055203 (2024).
[26]E. Walter, J. P. Farmer, M. S. Weidl, A. Pukhov, and F. Jenko, "Wakefield-driven filamentation of warm beams in plasma," arXiv:2406.07977 (2024).
[27]J. Chappell, A. C. Caldwell, and M. Wing, "A compact electron injector for the EIC based on plasma wakefields driven by the RHIC-EIC proton beam," arXiv:1907.01191 (2019).
[28]A. Caldwell, K. Lotov, A. Pukhov, and F. Simon, "Proton-driven plasma-wakefield acceleration," Nat. Phys. **5**, 363–367 (2009).
[29]G. Xia, O. Mete, A. Aimidula, C. P. Welsch, S. Chattopadhyay, S. Mandry, and M. Wing, "Collider design issues based on proton-driven plasma wakefield acceleration," Nucl. Instrum. Methods Phys. Res. A **740**, 173–179 (2014).
[30]N. Kumar, A. Pukhov, and K. Lotov, "Self-modulation instability of a long proton bunch in plasmas," Phys. Rev. Lett. **104**, 255003 (2010).
[31]M. Turner, P. Muggli, E. Adli, R. Agnello, M. Aladi, Y. Andrebe, O. Apsimon, R. Apsimon, A.-M. Bachmann, M. A. Baistrukov, AWAKE Collaboration *et al.*, "Experimental study of wakefields driven by a self-modulating proton bunch in plasma," Phys. Rev. Accel. Beams **23**, 081302 (2020).
[32]B. Allen, V. Yakimenko, M. Babzien, M. Fedurin, K. Kusche, and P. Muggli, "Experimental study of current filamentation instability," Phys. Rev. Lett. **109**, 185007 (2012).
[33]A. Pukhov, "Three-dimensional electromagnetic relativistic particle-in-cell code VLPL (Virtual Laser Plasma Lab)," J. Plasma Phys. **61**, 425–433 (1999).
[34]V. K. B. Olsen, E. Adli, and P. Muggli, "Emittance preservation of an electron beam in a loaded quasilinear plasma wakefield," Phys. Rev. Accel. Beams **21**, 011301 (2018).
[35]W. Lu, C. Huang, M. M. Zhou, W. B. Mori, and T. Katsouleas, "Limits of linear plasma wakefield theory for electron or positron beams," Phys. Plasmas **12**, 063101 (2005).
[36]K. V. Lotov, "Excitation of two-dimensional plasma wakefields by trains of equidistant particle bunches," Phys. Plasmas **20**, 083119 (2013).
[37]J. P. Farmer and G. Z. D. Porta, "Wakefield regeneration in a plasma accelerator," arXiv:2404.14175 (2024).
[38]K. Lotov and V. Minakov, "Proton beam self-modulation seeded by electron bunch in plasma with density ramp," Plasma Phys. Controlled Fusion **62**, 115025 (2020).
[39]J. B. Rosenzweig, G. Andonian, M. Ferrario, P. Muggli, O. Williams, V. Yakimenko, and K. Xuan, "Plasma wakefields in the quasi-nonlinear regime," AIP Conf. Proc. **1299**, 500–504 (2010).
[40]M. D. Litos, R. Ariniello, C. E. Doss, K. Hunt-Stone, and J. R. Cary, "Beam emittance preservation using Gaussian density ramps in a beam-driven plasma wakefield accelerator," Philos. Trans. R. Soc. A **377**, 20180181 (2019).
[41]C. Lindstrøm and M. Thévenet, "Emittance preservation in advanced accelerators," J. Instrum. **17**, P05016 (2022).
[42]M. Kozlova, I. Andriyash, J. Gautier, S. Sebban, S. Smartsev, N. Jourdain, U. Chaulagain, Y. Azamoum, A. Tafzi, J.-P. Goddet *et al.*, "Hard X rays from laser-wakefield accelerators in density tailored plasmas," Phys. Rev. X **10**, 011061 (2020).
[43]S. Fourmaux, E. Hallin, U. Chaulagain, S. Weber, and J. C. Kieffer, "Laser-based synchrotron X-ray radiation experimental scaling," Opt. Express **28**, 3147–3158 (2020).
[44]A. J. Gonsalves, K. Nakamura, J. Daniels, C. Benedetti, C. Pieronek, T. C. H. de Raadt, S. Steinke, J. H. Bin, S. S. Bulanov, J. van Tilborg *et al.*, "Petawatt laser guiding and electron beam acceleration to 8 GeV in a laser-heated capillary discharge waveguide," Phys. Rev. Lett. **122**, 084801 (2019).
[45]B. Miao, J. E. Shrock, L. Feder, R. C. Hollinger, J. Morrison, R. Nedbailo, A. Picksley, H. Song, S. Wang, J. J. Rocca *et al.*, "Multi-GeV electron bunches from an all-optical laser wakefield accelerator," Phys. Rev. X **12**, 031038 (2022).
[46]C. Aniculaesei, T. Ha, S. Yoffe, L. Labun, S. Milton, E. McCary, M. M. Spinks, H. J. Quevedo, O. Z. Labun, R. Sain *et al.*, "The acceleration of a high-charge electron bunch to 10 GeV in a 10-cm nanoparticle-assisted wakefield accelerator," Matter Radiat. Extremes **9**, 014001 (2024).